

Gamma-Ray Burst Spectral Evolution Through Crosscorrelations of Discriminator Light Curves

David L. Band

CASS 0424, University of California, San Diego, La Jolla, CA 92093

Received 1997 March 4; accepted 1997 April 21

To appear in the 1997 September 10 issue of
The Astrophysical Journal (Volume 486)

ABSTRACT

Gamma-ray burst spectra usually show hard-to-soft evolution within intensity spikes and from spike to spike. The techniques used to study spectral evolution often lack sufficient temporal resolution to determine the nature of this evolution. By comparing the auto- and crosscorrelations between the time histories of the BATSE Large Area Detector discriminator rates I have characterized the spectral evolution of a sample of 209 bursts. I find that hard-to-soft evolution is ubiquitous, and only $\sim 10\%$ of the bursts show clear soft-to-hard evolution.

Subject headings: gamma-rays: bursts

1. Introduction

Gamma-ray burst spectra are not constant during a burst, but tend to soften as the burst progresses. Since the observed spectrum reflects the energy content and particle distributions within the source's emitting region, spectral variations are an important diagnostic of the nature of this region. Until the origin of bursts is known definitively, the physics of the emission region will not be understood fully, and many burst phenomena will not be explained. Indeed, theory currently provides little guidance for the analysis of burst data. Nonetheless, the temporal and spectral properties of bursts might reveal clues about the origin of these events, and will provide powerful constraints on the detailed physical models which will be constructed when the sources are identified.

Spectral evolution has usually been demonstrated by fitting series of spectra accumulated during the burst. These studies (e.g., Kargatis et al. 1994; Ford et al.

1995) often lack the temporal resolution to characterize the spectral evolution of the short timescale structure which is evident to the eye in burst time histories. Here I introduce and use a method which sacrifices spectral resolution to gain the temporal resolution necessary to determine the character of the spectral evolution of a large burst sample. In this study I use the terms hard and soft to refer to high and low average photon energies, respectively.

Early studies revealed two basic characteristics of spectral evolution. By comparing the rates from two Konus detectors on *Venera* 11 and 12 covering different energy ranges, Golenetskii et al. (1984) reported that burst intensities and spectral hardness were correlated; thus when the intensity increased, the spectrum hardened. On the other hand, Norris et al. (1986) found a hard-to-soft trend across 10 bursts observed by GRS and HXRBS on the *Solar Maximum Mission*. Subsequent studies showed that both trends hold in general: the spectrum does indeed harden during intensity spikes, but there is a hard-to-soft trend during these spikes, and the hardness tends to peak at successively lower values from spike to spike (Kargatis et al. 1994 using SIGNE observations; Ford et al. 1995 using BATSE spectra). These studies lacked sufficient spectral and temporal resolution to determine how ubiquitous these spectral evolution trends are. Most of the earlier studies tracked the spectral evolution by fitting models to a sequence of spectra across a number of bursts, and then comparing the time histories of the intensity and a measure of the spectral hardness, e.g., the energy E_p of the peak of $E^2N(E) \propto \nu F_\nu$. However, counts must be collected over timescales of order seconds to accumulate a spectrum which can be fitted well; indeed, although the BATSE Spectroscopy Detectors (SDs) can accumulate spectra on a timescale as short as 0.128s, the temporal resolution frequently must be degraded to get a fit which determines the spectral parameters with relatively small uncertainties (Ford et al. 1995). However, the time history often shows temporal structure on timescales comparable to or shorter than the spectra’s accumulation times. Thus these studies often cannot determine the spectral trends of this short timescale structure.

Spectral resolution must be sacrificed to determine the spectral evolution on the timescales of the structure evident in a burst’s light curve. In general spectral fits are used to generate a single hardness value whose time history is compared to that of the intensity. Thus spectral evolution can be studied by cruder measures of spectral hardness available on shorter timescales. The BATSE Large Area Detectors (LADs) provide discriminator rates every 64 ms from 2.048 s before the burst trigger until 4–10 minutes after the trigger; background rates accumulated every 1.024 s are available for 10 minutes before this burst data. The discriminator rates are available for 4 channels covering 20–50 keV, 50–100 keV, 100–300 keV and 300 keV to approximately 2 MeV. These rates have excellent statistics since they are collected over wide energy bands from two or three LADs with their enormous areas of 2025 cm² each. Spectral evolution can be determined by comparing the light curves

of each discriminator channel. Indeed, spectral evolution is often clearly evident to the eye; in multispikes bursts the later spikes are frequently much weaker in the highest energy discriminator than in the lower energy discriminators.

Throughout this paper I refer to coherent increases and decreases in the light curve as spikes. While such structures are apparent to the eye, defining a spike quantitatively is complicated. For example, Norris et al. (1996) decompose burst light curves into pulses described by a 5 parameter functional form. Pendleton et al. (1997) use a peak-identification algorithm based on the depth of the minima between peaks. Here I do not use a rigorous definition of a spike but instead rely on a qualitative identification. Note that the bursts used in my analysis are strong and a statistical fluctuation will not be mistaken for a real spike.

The comparison of discriminator rates can reveal relative changes in spectral hardness within a burst. However, because the discriminators provide only 4 channels over broad energy bands from detectors with fairly poor spectral resolution (30% at 88 keV), the spectra (and therefore E_p) cannot be deconvolved from these rates. Many techniques of comparing these discriminator rates suggest themselves. For example, one can contrast the time histories of the intensity and various “colors,” ratios of the discriminator rates. Similarly, the “orbit” described by a burst in the multidimensional space defined by the discriminator rates can be studied. Here I use the crosscorrelation functions (CCFs) between different discriminator rates to characterize the spectral evolution of a large burst sample (note that the autocorrelation function—ACF—is the CCF of a rate with itself). As will be discussed in greater detail below, the graphical comparison of the CCFs of a fiducial channel with all the channels can be readily interpreted. For small lags the two time series will have been shifted relative to each other by very little, revealing the structure of the burst’s spikes. For multispikes bursts large lags will shift a spike in one time series to another spike in the second time series, permitting the comparison of the relative hardness of successive spikes.

Standard temporal analysis methods assume that the signal is “stationary,” that basic quantities which characterize the signal, such as the mean value or the frequency content, remain constant (e.g., Priestley 1981). These techniques assume that the finite time series under analysis is representative of the infinite time series from which the sample has been extracted. This is definitely not the case for gamma-ray bursts. These are transient events which can be studied in their entirety. In addition, the character of the burst changes as the burst progresses: the average intensity often decreases, and the spectrum usually softens. ACFs and CCFs do not assume underlying periodicities, and as I shall explain in §2, as defined for transient events, the ACFs and CCFs calculated with varying amounts

of background data are the same (except for statistical fluctuations). On the other hand, the ACFs and CCFs are averages over the entire burst and therefore assume that the relationship between quantities separated by a given timescale (lag) is the same throughout the burst. Other techniques, such as wavelets or pulse decomposition (Norris et al. 1996), are necessary to study how the structure at a given timescale changes over the burst.

ACFs and related quantities have been used before in the study of gamma-ray bursts, primarily to study the duration of temporal structure at different energies (which is a consequence of spectral evolution, although this evolution was not the purpose of most of these studies). Link, Epstein and Priedhorsky (1993) used the ACFs of the four LAD discriminator channels for 20 bursts to show that the duration of temporal structures within a burst decreases for higher energies; this was demonstrated quantitatively by integrating and comparing the area under the ACF curves. Their analysis did not distinguish between the structure on different timescales. Using the skewness function (related to the third moment of the time history) they also showed that bursts are asymmetric: they rise more rapidly than they fall. Nemiroff et al. (1994) confirmed that bursts are asymmetric. Fenimore et al. (1995) averaged the ACFs in each of the LAD discriminator channels of 45 bright bursts to find the average ACF as a function of energy. They found that the width of the temporal structure decreases with increasing energy as a power law $E^{-0.4}$, and that the average ACF can be parameterized as the sum of two exponentials. In’t Zand and Fenimore (1996) analyzed the properties of burst ACFs in terms of a modified shot noise model, and concluded that there are no hidden systematic trends which preclude the use of ACFs to study the duration of temporal structure (e.g., possible cosmological time dilation). Kouveliotou et al. (1992) used a Fourier cross-spectral technique (using quantities which are Fourier transforms of the CCF) to show that the hard channels lead the soft channels in 90% of 22 bursts.

The calculation of CCFs for transient events involves some subtleties; the methodology is developed in §2. The interpretation of the resulting CCFs is explored in §3. Then I present the results of applying this technique to a large burst sample (§4). Finally, I discuss the implications of these results (§5).

2. Methodology

The CCF measures the temporal correlation of two time series v_1 and v_2 :

$$CCF(\tau; v_1, v_2) = \frac{\langle v_1(t)v_2(t + \tau) \rangle}{\sigma_{v1}\sigma_{v2}} \quad \text{where} \quad \sigma_v = \sqrt{\langle v^2 \rangle} \quad , \quad (1)$$

and τ is called the “lag.” If v_2 leads v_1 by t_0 (e.g., $v_1(t) = v_2(t - t_0)$) then the CCF peaks at $\tau = -t_0$. The ACF is the CCF of a time series with itself:

$$ACF(\tau; v) = CCF(\tau; v, v) \quad . \quad (2)$$

Note that the ACF is symmetrical, and that $ACF(\tau = 0; v) = 1$.

In most applications, the CCF is calculated for an infinitely long function $d(t)$ which is sampled over a short time range; the sample is assumed to be characteristic of all time ranges (i.e., the signal is assumed to be “stationary”). Since the interest is in the varying component of the signal, the signal is regarded as fluctuations around a constant value, and the CCF is calculated using a zero-mean time series:

$$v(t) = d(t) - \langle d(t) \rangle \quad (3)$$

However, a gamma-ray burst is a transient phenomenon which is contained entirely within the sampled time range. If the transient event were treated as a stationary event, the background rate before and after the burst would have a negative value in the zero-mean time series sampled over a finite sampling window and the calculated CCF would depend on the size of this window. A burst time series acquired with an infinite data window would have a mean equal to the background rate (if constant) since the counts in the burst would be diluted by the infinite time range, and the background in the zero-mean time series would fluctuate around zero. Therefore, I define the CCF using a background-subtracted time series

$$v(t) = d(t) - b(t) \quad (4)$$

which emphasizes the signal of interest (Link et al. 1993; Fenimore et al. 1995). Using this definition of $v(t)$ the difference between the CCFs calculated for the infinite and finite data windows should be small since the background omitted in the finite data window would have contributed nothing, on average, to all averages. Thus the effective data window can be considered to be greater than the time range actually sampled.

The observed signal $v(t)$ includes noise $n(t)$. We would like to find the ACF and CCF for the signal alone, mitigating the bias introduced by the presence of noise. I assume the noise has the following properties:

$$\langle n \rangle = 0 \quad \text{and} \quad \langle n(t)n(t + \tau) \rangle = \sigma_n^2 \delta(\tau) \quad . \quad (5)$$

Note that $\langle n(t)n(t + \tau) \rangle$ is truly 0 for $\tau \neq 0$ only for an infinite time series (or only on average), and I expect small fluctuations around 0 for any particular finite time series. The background-subtracted time series is the sum of the signal $s(t)$ and the noise $n(t)$,

$$v(t) = s(t) + n(t), \quad \text{and} \quad \sigma_v^2 = \sigma_s^2 + \sigma_n^2 + 2\langle sn \rangle \quad . \quad (6)$$

I do not consider the uncertainty in the determination of the background $b(t)$ which introduces an error which might violate both properties in eq. (5). The ACF calculated with σ_v is

$$ACF(\tau; v) = ACF(\tau; s) \frac{\sigma_s^2}{\sigma_v^2} + \frac{\sigma_n^2}{\sigma_v^2} \delta(\tau) + \frac{\langle n(t)s(t+\tau) + s(t)n(t+\tau) \rangle}{\sigma_v^2} \quad (7)$$

while the CCF is

$$\begin{aligned} CCF(\tau; v_1, v_2) &= CCF(\tau; s_1, s_2) \frac{\sigma_{s1}\sigma_{s2}}{\sigma_{v1}\sigma_{v2}} \\ &+ \frac{\langle n_1(t)n_2(t+\tau) \rangle}{\sigma_{v1}\sigma_{v2}} + \frac{\langle n_1(t)s_2(t+\tau) + s_1(t)n_2(t+\tau) \rangle}{\sigma_{v1}\sigma_{v2}} . \end{aligned} \quad (8)$$

On average I expect $\langle n_1(t)n_2(t+\tau) \rangle = 0$ and $\langle s(t)n(t+\tau) \rangle = 0$. If the magnitude of the noise n is a function of the signal s (e.g., n results from Poisson statistics for binned data), the average $\langle ns \rangle$ should be close to 0 because n has zero mean, although these averages will actually fluctuate around 0 because of the finite number of data points. Note that the noise reduces the signal's ACF and CCF, and produces a spike at zero lag in the ACF. To correct for this effect of noise, I change the variance used in the denominators of the ACF and CCF to

$$\sigma_v'^2 = \sigma_v^2 - \sigma_n^2 \quad (9)$$

(Link et al. 1993; Fenimore et al. 1995). For noisy signals this expression can underestimate the variance, and thus overestimate the CCF and ACF.

Since the time series is sampled at a number of discrete data points, averages are calculated by sums, not integrals. Assume there are N data points which correspond to the counts accumulated during time bins of duration $\Delta t = T/N$; the time series spans a time range T . I define the quantities as follows:

$$\begin{aligned} v_i &= d_i - b_i \quad , \\ \sigma_v'^2 &= \frac{1}{N} \sum_{i=1}^N (v_i^2 - d_i) \quad , \\ ACF(\tau = k\Delta t; v) &= \frac{\sum_{i=\max(1, 1-k)}^{\min(N, N-k)} v_i v_{i+k}}{N\sigma_v'^2} \quad , \\ CCF(\tau = k\Delta t; v_1, v_2) &= \frac{\sum_{i=\max(1, 1-k)}^{\min(N, N-k)} v_{1i} v_{2(i+k)}}{N\sqrt{\sigma_{v1}'\sigma_{v2}'}} \quad . \end{aligned} \quad (10)$$

For these discretized equations d_i is the observed data point from the i th time bin, b_i is the background rate (usually interpolated from data before and after the burst), and v_i is the

background-subtracted signal. If there are more than one time series, then v_{1i} is the i th data point of the first time series, etc. I have assumed that the noise results from Poisson fluctuations, and therefore $\sigma_n^2 = \langle d_i \rangle$. In the ACF and CCF there are $N - |k|$ products in each sum for a lag of $\tau = k\Delta t$, yet they are divided by N to form the average. As discussed above, I am effectively assuming that the products in the time range where one time series extends beyond the other are approximately zero, since at least one of the time series will be background over that time range. In the absence of noise the ACF and CCF will not change with variations in the amount of background data included before and after the burst. Similarly, $\sigma_v'^2$ should be independent of how much background is included since on average $v_i^2 \sim d_i$ for background data points. Yet $\sigma_v'^2$ will be sensitive to fluctuations and small errors in the background determination, and therefore the most accurate CCFs and ACFs are obtained by including only the burst within the data window.

A measure of the uncertainty is desirable for any observed or calculated quantity. The uncertainty on the ACFs and CCFs can be estimated by propagating the uncertainty on each element of the two time series (see also Fenimore et al. 1995). This calculation requires the partial derivatives of the ACF and CCF with respect to each time series element, an algebraically complicated quantity not presented here. The uncertainties in the ACF and CCF values at different lags are correlated both because the uncertainty in the normalization is a component of the overall uncertainty and because each ACF and CCF value is a function of each time series element. In general the uncertainties are small.

To study the effect of noise empirically, I calculated the ACF and CCFs for time series with different signal-to-noise ratios (SNRs), and found significant deviations only for low SNRs. For example, I computed the CCF for a ~ 1 s pulse where one time series was very strong and the second one was weak. I find significant deviations (the rising and falling segments of the CCF differ noticeably from the asymptotic value) when the peak time bin of the weak time series had an SNR less than 3 (the background count rate was 3000 cts s^{-1} , the time bins were 0.064 s wide and the signal/background at the peak was 0.24). Only for much smaller SNRs do the correlation curves become noisy. In practice the signal in the highest energy discriminator (300–2000 keV) was often very weak or nonexistent and the CCF with this discriminator channel was very noisy. In such cases I neglected the CCF with this channel in the analysis.

The discriminator time series are constructed from three different LAD data types—DISCLA, PREB and DISCSC (Fishman et al. 1989). The result has 1.024 s resolution up to 2.048 s before the burst trigger, and 0.064 s thereafter. The CCFs and ACFs are calculated with the minimum data necessary to include the burst. Occasionally the burst began more than 2.048 s before the trigger when the time bins were still 1.024 s wide rather

than 0.064 s. Since I want to include all the identifiable burst emission, and the ACF and CCF require data with uniform time bins, I replace each of these 1.024 s bins with 16 0.064 s bins with the same count rate. To insure that these new 0.064 s bins have the appropriate noise characteristics, I add Gaussian fluctuations. In general the background is fitted with a quadratic polynomial of time using background data before and after the burst. I calculate and plot the ACF for discriminator 3 (100–300 keV) and the CCFs for discriminators 1 (20–50 keV), 2 (50–100 keV) and 4 (300–~ 2000 keV) with discriminator 3, i.e., $ACF(\tau; v_3)$ and $CCF(\tau; v_3, v_1)$, $CCF(\tau; v_3, v_2)$, and $CCF(\tau; v_3, v_4)$. These four functions are then compared both graphically and quantitatively.

3. Interpretation of ACFs and CCFs

For every burst in my sample I calculate and plot the ACF for discriminator 3 and the CCFs for discriminators 1, 2 and 4 with discriminator 3. Thus the spectral evolution must be characterized from the differences between the ACF and the CCFs. Here I present a number of heuristic examples which reveal the features which can be extracted from the graphical comparison of these curves. In these examples I compare two time series, v_h and v_s , meant to represent high and low energy channels, respectively, and I calculate $ACF(\tau; v_h)$ and $CCF(\tau; v_h, v_s)$.

First, consider $v_h = \exp(-t/t_h)$ and $v_s = \exp(-t/t_s)$ for $t \geq 0$. If v_h and v_s are the hard and soft channels, respectively, then $t_s > t_h$ for hard-to-soft evolution. Consequently

$$ACF(\tau; v_h) = \exp(-|\tau|/t_h) \quad , \quad (11)$$

$$CCF(\tau; v_h, v_s) = \begin{cases} 2\frac{\sqrt{t_h t_s}}{t_h + t_s} \exp(-\tau/t_s) & , \quad \tau > 0 \\ 2\frac{\sqrt{t_h t_s}}{t_h + t_s} \exp(\tau/t_h) & , \quad \tau \leq 0 \end{cases} \quad . \quad (12)$$

Thus for hard-to-soft evolution of falling exponential spikes the CCF and ACF will be parallel on the negative lag side, while the CCF will decrease more slowly on the positive lag side. If t_s is not much larger than t_h (as is often the case), then the maximum CCF value is not much less than 1. Consequently the ACF and CCF will nearly coincide on the negative lag side, and the CCF will exceed the ACF on the positive lag side (see Figure 1a).

Now consider rising exponentials. In this case the ACF is the same as above, but the CCF is time reversed: $CCF \propto \exp(-t/t_h)$ for $\tau > 0$ and $CCF \propto \exp(t/t_s)$ for $\tau \leq 0$. However, now $t_s < t_h$ for hard-to-soft evolution: the CCF rises more rapidly than the ACF on the negative lag side, and is parallel to the ACF on the positive side (see Figure 1b).

These examples with exponential spikes demonstrate two features of the comparison between ACFs and CCFs. First, if the ACF is calculated for the hard channel, then

hard-to-soft evolution is indicated by the CCF rising more rapidly on the negative lag side or falling more slowly on the positive lag side than the ACF. Second, the relative widths of the ACF and CCF indicate the relative widths of the spike in the hard and soft channels.

However, the width of an ACF or CCF peak must be interpreted with care. Here I define the width to be the FWHM of the peak in the time series or ACF. The relation between the width in the time series and the ACF depends on the shape of the peak. For a square pulse of width Δt the $ACF = 1 - |\tau|/\Delta t$, and thus the signal and ACF widths are the same. For a triangular pulse (infinitesimal rise time, linear decay) of length Δt the $ACF = (1 - |\tau|/\Delta t)^2(1 + |\tau|/2\Delta t)$, and the ACF width is $\sim 4/3$ the pulse width. For a Gaussian pulse $v \propto \exp[-(t/\sigma)^2]$ the $ACF = \exp[-t^2/2\sigma^2]$, and thus the ACF width is $\sqrt{2}$ times the pulse width. Finally, as shown above, an exponential pulse has an ACF with a width twice that of the signal. The actual profiles of spikes in bursts are complicated, and therefore the widths of the ACFs, and by analogy the CCFs, cannot be translated quantitatively into measures of the spike widths.

To interpret well-separated secondary peaks in the ACF and CCF when the lag is great enough so that different spikes coincide, consider a burst which consists of two spikes of unit width. Without loss of generality the height of the first peak in each time series can be set to unity. Then $v_h(t) = \delta(t) + a_h\delta(t - \Delta t)$ and $v_s(t) = \delta(t) + a_s\delta(t - \Delta t)$, where Δt is the separation between peaks. Hard-to-soft evolution from spike to spike results from $a_s > a_h$; it does not matter whether a_s or a_h are greater than 1. The ACF of v_h is

$$ACF(\tau; v_h) = \delta(\tau) + \frac{a_h}{1 + a_h^2} \delta(\tau \pm \Delta t) \quad (13)$$

and the CCF of v_h and v_s is

$$CCF(\tau; v_h, v_s) = \frac{1 + a_h a_s}{\sqrt{(1 + a_h^2)(1 + a_s^2)}} \delta(\tau) + \frac{a_h}{1 + a_h^2} \sqrt{\frac{1 + a_h^2}{1 + a_s^2}} \left(\delta(\tau + \Delta t) + \frac{a_s}{a_h} \delta(\tau - \Delta t) \right) \quad (14)$$

If $a_s > a_h$ then the CCF will be greater than the ACF at $\tau = \Delta t$. The comparative heights of the secondary peaks in the ACF and CCF on the positive lag side indicates the relative magnitudes of a_s and a_h , and thus the nature of the spike-to-spike spectral evolution.

I conclude that for the ACFs and CCFs calculated from the BATSE data, hard-to-soft evolution is indicated by $CCF(\tau; v_3, v_4) < ACF(\tau; v_3) < CCF(\tau; v_3, v_2) < CCF(\tau; v_3, v_1)$ on the positive lag side or the opposite on the negative lag side.

4. Results

My burst sample consists of 209 of the strongest BATSE bursts from the beginning of the mission through 15 August 1996. In general, the bursts had a peak count rate in the 50–300 keV band greater than $10,000 \text{ cts s}^{-1}$, but some large fluence bursts with a smaller peak count rate were included. Almost all the bursts I selected were longer than 1 s so that there would be enough points to produce ACFs and CCFs with structure. Consequently this burst sample is not statistically complete. Because of the preference for long, strong bursts, many of the bursts consisted of several clusters of emissions separated by periods of little or no emission above background.

Figure 2 shows six bursts: the upper panel is the time history summing all the discriminator channels, and the bottom panel is a comparison of the $CCF(\tau; v_3, v_4)$ (3 dots-dashed curve), $ACF(\tau; v_3)$ (solid curve), $CCF(\tau; v_3, v_2)$ (dot-dashed curve), and $CCF(\tau; v_3, v_1)$ (dashed curve). The order and relative widths of $CCF(\tau; v_3, v_4)$, $ACF(\tau; v_3)$, $CCF(\tau; v_3, v_2)$, and $CCF(\tau; v_3, v_1)$ on the positive lag side of bursts 3B 910503, 3B 911118, and 3B 920216 show that these bursts underwent hard-to-soft evolution (bursts are identified by their names in the 3B Catalog of Meegan et al. (1996), except for bursts which occurred after this catalog). In particular, $CCF(\tau; v_3, v_4) < ACF(\tau; v_3) < CCF(\tau; v_3, v_2) < CCF(\tau; v_3, v_1)$ in the secondary structure at $\tau = 40\text{--}50 \text{ s}$ of the correlations for 3B 910503 indicate that the first emission cluster of this burst at $t = 0\text{--}10 \text{ s}$ was harder than the second cluster at $t = 46\text{--}54 \text{ s}$. On the other hand 3B 920701 and 3B 930612B are among the very rare cases of soft-to-hard evolution; note that the order of the correlations is reversed compared to the usual hard-to-soft evolution. Finally, GB 941119 is an example of a burst without clear evolution.

Emission spikes or clusters of spikes which are well-separated (e.g., separations many times their width) result in correlations with structure that can clearly be identified as the correlation of a cluster with itself (around zero lag) or with other clusters, as is the case for 3B 910503. On the other hand, the correlations may smooth over the structure within a cluster of closely spaced spikes (e.g., spacing of order the width of a spike); again, the central peak of the correlations for 3B 910503 is such an example. While there may be clear short duration emission spikes ($\sim 1 \text{ s}$ long), the central ACF and CCF peaks are often much broader, as is the case for 3B 9110503 and GB 941119. Thus, if many emission spikes occur in a cluster, then the width of the ACFs' and CCFs' central peak may reflect the duration of the cluster, and not of the individual spikes.

Hard-to-soft spectral evolution is found in most bursts. I categorized the spectral evolution evident in the central and secondary peaks in the ACFs and CCFs. To those bursts which show unambiguous hard-to-soft or soft-to-hard evolution I assigned a value

of +2 or -2, respectively. Note that the evolution need not be extreme for a value of ± 2 . Where the signature for spectral evolution was somewhat ambiguous I assigned ± 1 . Finally, I gave a 0 to those bursts with no indication of spectral evolution. Thus positive and negative values indicate hard-to-soft and soft-to-hard evolution, respectively, and the magnitude denotes the confidence with which I could determine the trend. I assigned values for both the central peak and the secondary structure. The results of this analysis are tabulated in Table 1; since there are just over 200 bursts in my sample, each burst corresponds to approximately 0.5% of the sample. In 9 cases the secondary structure showed both types of evolution, in which case I split the burst between the two types of evolution. If the burst was very simple and there was no secondary structure, I assigned to the secondary structure the same value as the central peak. As is clear from the table, hard-to-soft spectral evolution is a standard characteristic of gamma-ray bursts. However, there are bursts with soft-to-hard evolution, although only $\sim 2\%$ show such evolution in both the central peak and the secondary structure. Soft-to-hard evolution is more common in the secondary structure than in the central peak.

The evolutionary trend in the central peak can be determined quantitatively by considering the time lag of the peaks of the CCFs, as are shown by the cumulative distributions in Figure 3. These lags are related to the time shifts found by Kouveliotou et al. (1992) using cross Fourier transforms (which are the transforms of CCFs). As is clear, the CCFs of the higher energy channels peak before those of lower energies, typically by ~ 0.1 s, indicating that the light curve at higher energies peaks earlier than at lower energies. Similarly, the CCFs for the lower energy channels are broader than for higher energies. Figure 4 shows the cumulative distribution of the ratios of the CCFs and the ACF at a correlation value of 0.5; the differences in the width are typically $\sim 20\%$.

Attempts to characterize burst morphology have generally been unsuccessful. One apparent class consists of FREDs—Fast Rise, Exponential Decays—whose name describes them. My database includes 35 FREDs or similarly simple bursts, nine bursts which appear to consist of two or more FREDs and one case of an “inverse FRED.” With one exception (GB 930612B, included in Figure 2) which has more structure than the standard FRED, all these bursts show unambiguous hard-to-soft evolution, although not necessarily between FREDs in a multi-FRED burst. Similarly, Bhat et al. (1994) found that hard-to-soft evolution predominates in FREDs; they also report that the high energies lead the low energies by a time proportional to the FRED’s rise time. Note that Norris et al. (1996) found a similar trend between pulses resulting from deconvolving the LAD light curves.

Many bursts have well separated “clumps” of emission, and in many cases the character of these clumps differs within a burst: some consist of spikes which barely overlap,

whereas others have a few spikes which protrude from a smooth envelope. This type of characterization remains to be quantified. By comparing the ACFs and CCFs at both positive and negative lags I find that in some bursts one emission clump shows very marked spectral evolution whereas a second shows very little. Although these phenomena need to be explored further, they suggest that there are qualitatively different emission processes which can occur within the same burst.

5. Discussion

My analysis of the ACFs and CCFs of a sample of strong bursts shows that within individual spikes or clusters of spikes, $\sim 90\%$ of the bursts show hard-to-soft evolution and in only $\sim 3\%$ is the opposite trend evident. Similarly, hard-to-soft evolution from spike to spike or among successive clusters of spikes characterizes $\sim 80\%$ of the bursts, while $\sim 15\%$ show the opposite trend. Thus hard-to-soft evolution is a very common feature of gamma-ray bursts, but counterexamples exist. This feature of burst phenomenology must ultimately be explained by any successful burst model.

For example, in the current fireball models a relativistically expanding fireball radiates at the shocks formed either as the ejecta within the fireball plows into the surrounding medium (Rees & Mészáros 1992; Mészáros & Rees 1993; Mészáros, Rees & Papathanssiou 1994; Katz 1994; Sari, Narayan & Piran 1996) or as a consequence of inhomogeneities within the expanding fireball (Rees & Mészáros 1994; Paczyński & Xu 1994; Papathanssiou & Mészáros 1996). At an external shock multiple spikes result from energy release events which cool on a timescale short compared to the expansion (Sari et al. 1996). The Lorentz factor of the external shock should drop as the fireball expands and the external medium is swept up. Spike-to-spike spectral evolution can be explained easily by later energy release events occurring at larger fireball radii. However, internal shock models attribute multiple, well-separated spikes to the shocks which form at different times and radii as inhomogeneities in the flow within the fireball cause different regions to collide; for such models it is not obvious why there should be a hard-to-soft trend from spike to spike. Whether the electron acceleration event occurs at an internal or external shock, the spectral evolution resulting from the electron cooling must be reconciled with the observations.

Detailed physical implications of spectral evolution are model dependent (e.g., the above discussion of the fireball scenarios) but some general conclusions are possible. That the average photon energy increases when the photon flux increases suggests that energy has been injected into the emission region, increasing the average energy of the emitting particles. The hard-to-soft trend from spike to spike indicates that if there is one emission

region, it retains a memory of previous emission events. If there are multiple regions, they may communicate, or alternatively, independent regions may possess similar internal “clocks” such that they emit softer spikes later in the burst.

The ACF and CCF methodology can be extended to address deficiencies in the current study. First, the ACFs and CCFs assume that the correlation between quantities with a given time separation is the same throughout the burst. Therefore the ACFs and CCFs of individual spikes and clusters of spikes within a burst can be calculated separately to characterize their spectral evolution. Structure in different parts of a burst frequently appears very different. For example, 3B 910503 (see Figure 2) begins with a cluster of spikes while the emission which begins 45 s after the burst trigger is much smoother and simpler; thus the ACFs and CCFs of the two emission clusters can be compared. Presumably the temporal and spectral structure reflects the processes by which the emission region is energized and radiates.

Second, when intensity spikes occur in clusters where the separation between spikes is comparable to the width of the spikes, the effect of the spikes’ structure cannot be separated from that of the overall cluster. Filtering the time history (e.g., using an FFT filter or wavelets) before calculating the ACFs and CCFs may separate the structure on different timescales. This combination of filtering and CCFs has been applied to solar flares (e.g., Aschwanden et al. 1996).

Third, I restricted myself to bursts with durations over 1 s because of the 0.064 s time resolution of the LAD light curves I used. Greater time resolution can be obtained from the TTE data type (which provides the time necessary to accumulate a given number of counts) for bright bursts. Although it would have to be modified (the TTE rates are not provided on a uniform grid), the methodology presented here can be applied to the TTE data to study the spectral evolution of short bursts.

6. Summary

Spectral evolution can be characterized by comparing the crosscorrelations of a fiducial burst intensity light curve with the light curves in different energy bands. The structure of the crosscorrelations in the peak around zero lag results from the spectral evolution of individual intensity spikes or clusters of spikes. Secondary peaks in the crosscorrelations away from zero lag result from well-separated spikes or clusters of spikes. Thus the structure of the crosscorrelations at these secondary peaks characterize the peak-to-peak spectral evolution.

I applied this crosscorrelation technique to a sample of 209 bursts observed by BATSE using rates from the 4 LAD discriminator channels. My fiducial light curve was the count rate in the 100–300 keV band. I find hard-to-soft evolution is common, although there are a few counterexamples. The preference for hard-to-soft evolution is somewhat stronger for individual spikes and clusters of spikes than for well-separated structure. The shift in the centers of the peaks around zero lag between the crosscorrelations with low energy (20–50 keV) and high energy (300–2000 keV) channels is of order 0.1 s.

I thank my collaborators on the BATSE team for their assistance over the past few years. In addition, I am grateful for the careful reading of this paper by the referee, J. Norris, which has improved the text’s clarity. BATSE research at UCSD is supported by NASA contract NAS8-36081.

REFERENCES

- Aschwanden, M. J., et al. 1996, *ApJ*, 468, 398
- Bhat, N. P., et al. 1994, *ApJ*, 426, 604
- Fishman, G., et al. 1989, in *Proc. Gamma Ray Observatory Science Workshop*, ed. W. N. Johnson (Washington: NASA), 2-39
- Fenimore, E. E., Zand, J. J. M. In’t, Norris, J. P., Bonnell, J. T., and Nemiroff, R. J. 1995, *ApJ*, 448, L101
- Ford, L., et al. 1995, *ApJ*, 439, 307
- Golenetskii, S. V., et al. 1984, *Nature*, 306, 451
- In’t Zand, J. J. M, and Fenimore, E. E. 1996, *ApJ*, 464, 622
- Kargatis, V. E., Liang, E. P., Hurley, K. C., Barat C., Eveno, E., and Niel, M. 1994, *ApJ*, 422, 260
- Katz, J. I. 1994, *ApJ*, 432, L107
- Kouveliotou, C., et al. 1992, in *Gamma-Ray Bursts, AIP Conf. Proc. 265*, eds., W. S. Paciesas and G. J. Fishman (New York: AIP), 299
- Link, B., Epstein, R. I., and Priedhorsky, W. C. 1993, *ApJ*, 408, L81

- Meegan, C. A., Fishman, G. J., Wilson, R. B., Paciasas, W. S., Pendleton, G. N., Horack, J. M., Brock, M. N., & Kouveliotou, C. 1992, *Nature*, 355, 143
- Meegan, C. A., et al. 1996, *ApJS*, 106, 65
- Mészáros, P. & Rees, M. 1993, *ApJ*, 405, 278
- Mészáros, P., Rees, M. & Papathanssiou, H. 1994, *ApJ*, 432, 181
- Nemiroff, R., et al. 1994, *ApJ*, 423, 432
- Norris, J. P., et al. 1986, *ApJ*, 301, 213
- Norris, J. P., et al. 1996, *ApJ*, 459, 393
- Paczynski, B. & Xu, G. 1994, *ApJ*, 427, 708
- Papathanssiou, H., & Mészáros, P. 1996, *ApJ*, 471, L91
- Pendleton, G., et al. 1997, *ApJ*, submitted
- Priestley, M. B. 1981, *Spectral Analysis and Time Series* (London: Academic Press)
- Rees, M. & Mészáros, P. 1992, *MNRAS*, 258, 41P
- Rees, M. & Mészáros, P. 1994, *ApJ*, 430, L93
- Sari, R., Narayan, R. & Piran, T. 1996, *ApJ*, 473, 204

Fig. 1.— $ACF(\tau; v_h)$ (solid curve) and $CCF(\tau; v_h, v_s)$ (dashed curve) for exponential spikes. In panel (a) the spikes are falling exponentials $v_{h,s} \propto \exp(-t/t_{h,s})$ for $t \geq 0$ with $t_h = 1$ and $t_s = 1.5$, while in panel (b) the spikes are rising exponentials $v_{h,s} \propto \exp(t/t_{h,s})$ for $t \leq 0$ with $t_h = 1$ and $t_s = 2/3$. Thus both cases are characterized by hard-to-soft spectral evolution.

Fig. 2.— Intensity time history (top panel) and correlation functions (bottom panel) for 6 bursts. The intensity is summed over the 4 LAD discriminators, covering 20–2000 keV. Extending over the time range included in the correlation functions, the (nearly) horizontal line in the time history plot is the calculated background rate. The correlation functions are $CCF(\tau; v_3, v_4)$ (the CCF of LAD discriminator 3 with discriminator 4—3 dots-dashed curve), $ACF(\tau; v_3)$ (the ACF of discriminator 3—solid curve), $CCF(\tau; v_3, v_2)$ (discriminator 3 with discriminator 2—dot-dashed curve), and $CCF(\tau; v_3, v_1)$ (discriminator 3 with discriminator 1—dashed curve). In general, hard-to-soft evolution is indicated by $CCF(\tau; v_3, v_4) < ACF(\tau; v_3) < CCF(\tau; v_3, v_2) < CCF(\tau; v_3, v_1)$ on the positive lag side.

Fig. 3.— Cumulative distributions of the lags of the center of the central peak. The curves are for $CCF(\tau; v_3, v_4)$ (3 dots-dashed curve), $ACF(\tau; v_3)$ (solid curve—the ACF defines zero lag), $CCF(\tau; v_3, v_2)$ (dashed curve), and $CCF(\tau; v_3, v_1)$ (dot-dashed curve). The plot shows that on average the higher energy light curves peak earlier than the lower energy light curves.

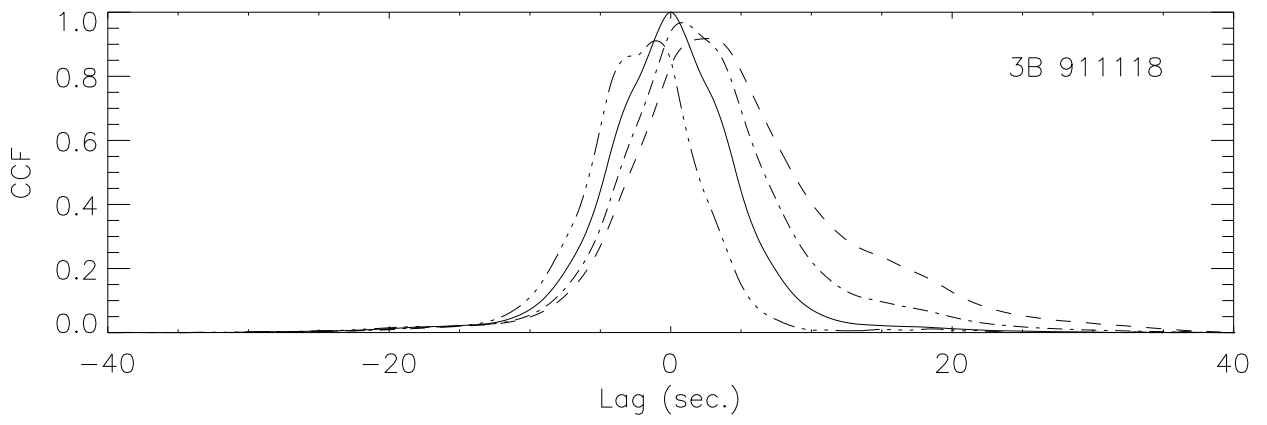
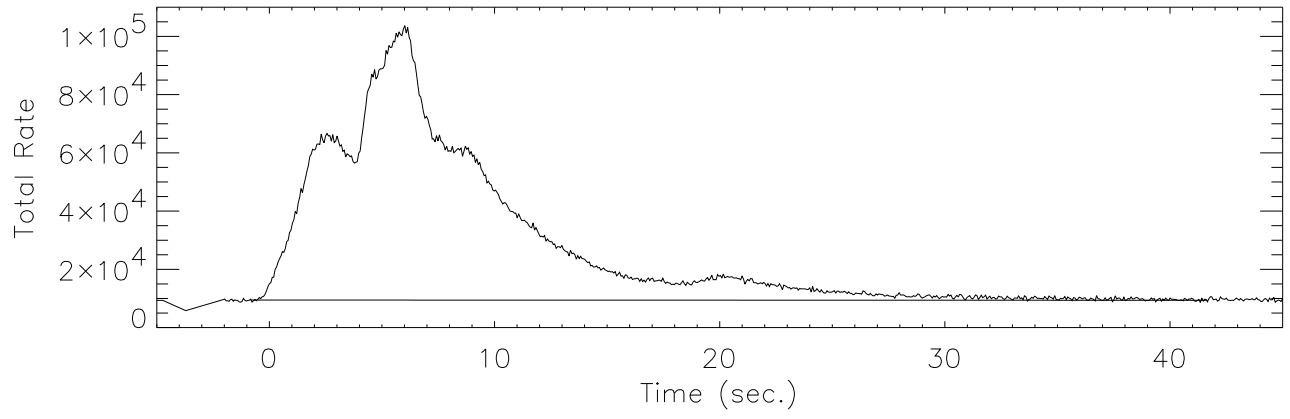
Fig. 4.— Cumulative distributions of the ratio of the CCF to ACF widths at a correlation value of 0.5. The curves are for $CCF(\tau; v_3, v_4)/ACF(\tau; v_3)$ (3 dots-dashed curve), $CCF(\tau; v_3, v_2)/ACF(\tau; v_3)$ (dashed curve), and $CCF(\tau; v_3, v_1)/ACF(\tau; v_3)$ (dot-dashed curve). The plot shows that on average the lower energy light curves are broader than the higher energy light curves.

Table 1. Spectral Evolution of the Central Peak and the Secondary Structure

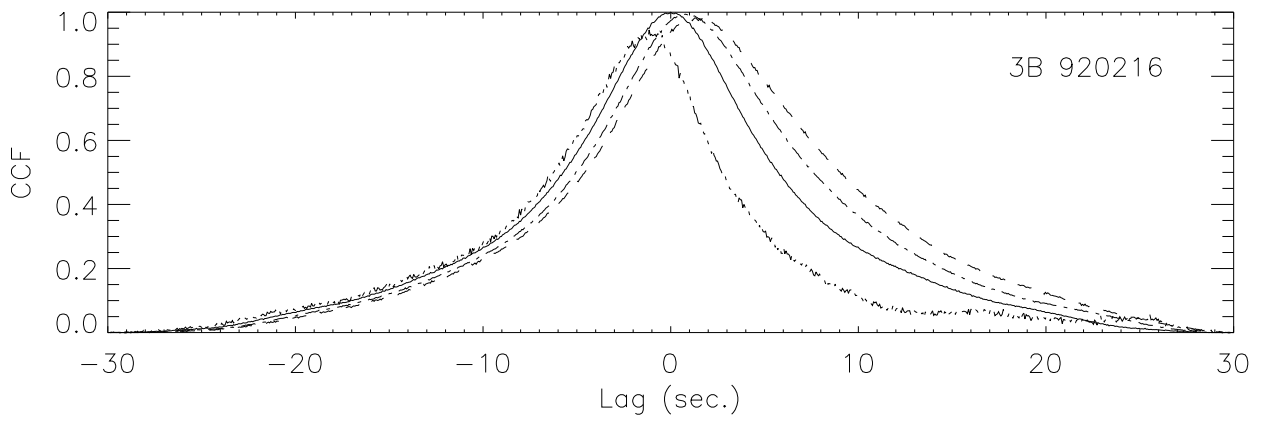
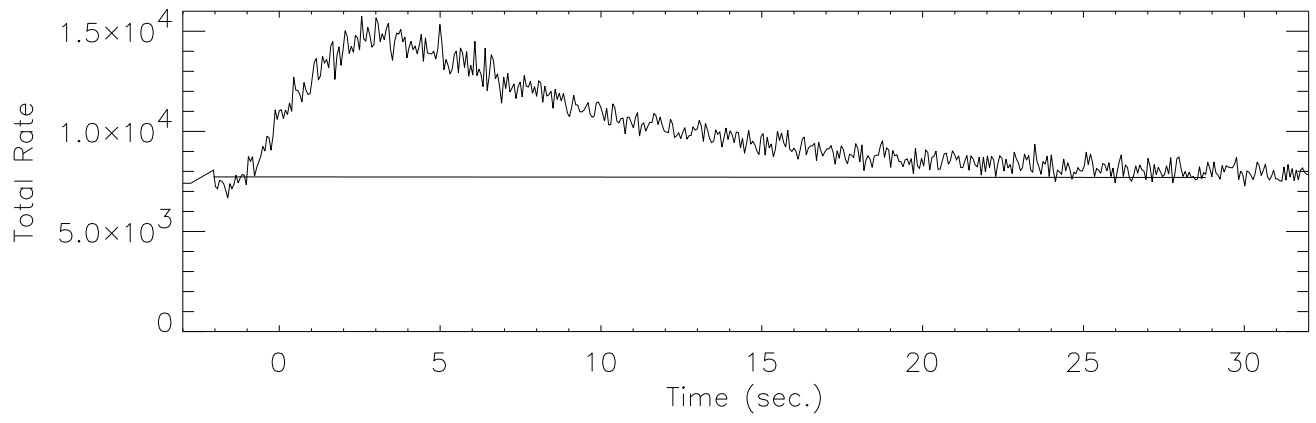
		Central Peak					Total
		-2	-1	0	+1	+2	
Secondary Structure	+2	2	1	8	16.5	121	148.5
	+1	0	0	0	8	8	16
	0	0	0	1	6	9	16
	-1	0	1	2	2	5.5	10.5
	-2	3	0	2	2.5	10.5	18
Total		5	2	13	35	154	209

Note. — Positive and negative values indicate hard-to-soft and soft-to-hard evolution, respectively. A magnitude of 2 was assigned when the evolution was unambiguous, while a magnitude of 1 indicates ambiguity. The absence of apparent evolution resulted in value of 0. If the secondary structure showed both types of evolution, half the burst was assigned to each category. Note that the value does not indicate whether the spectral evolution is extreme.

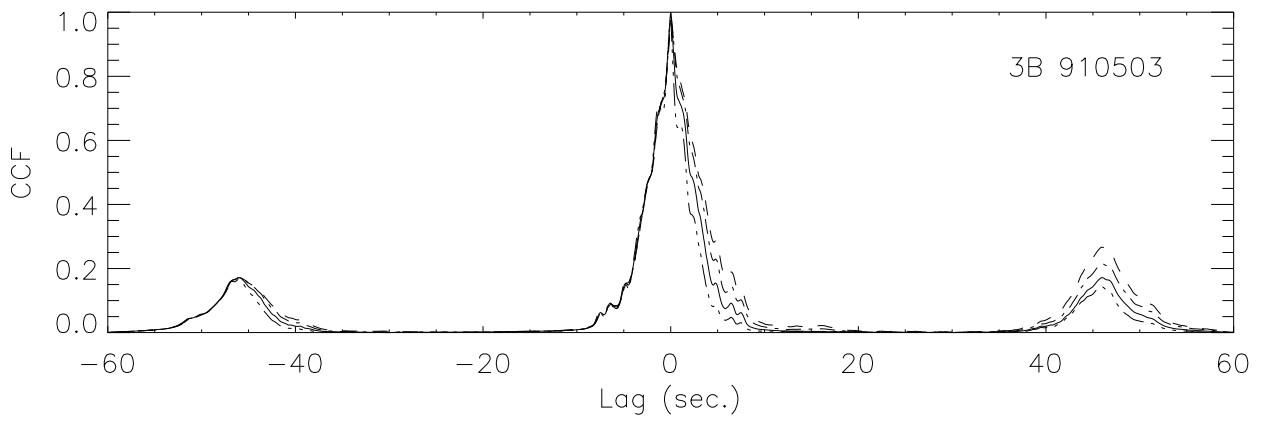
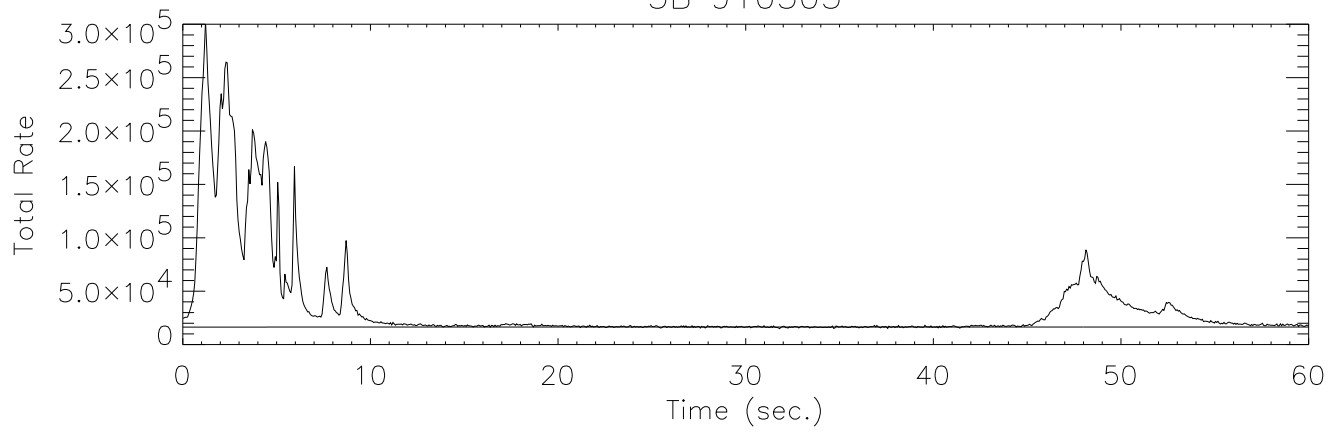
3B 911118

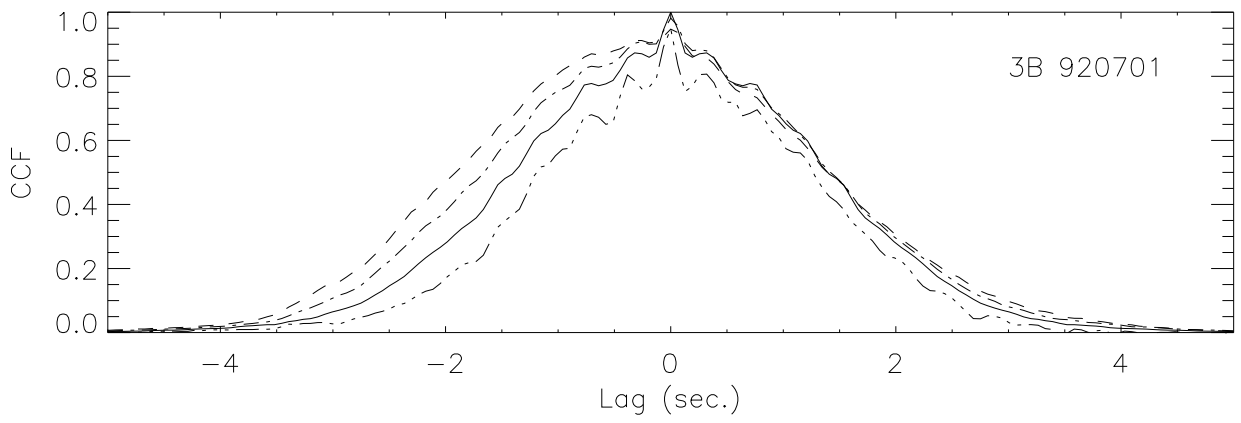
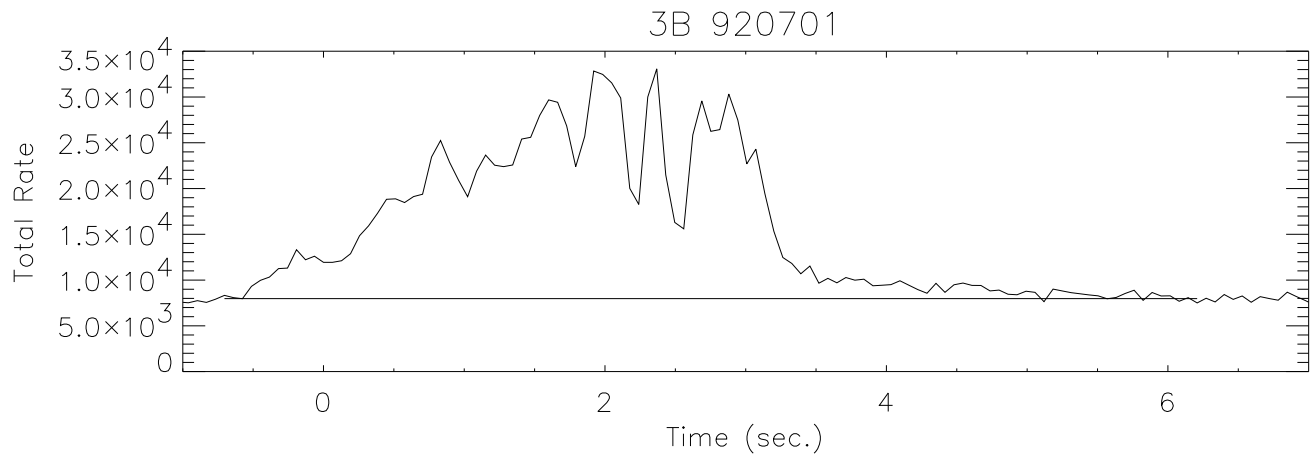


3B 920216

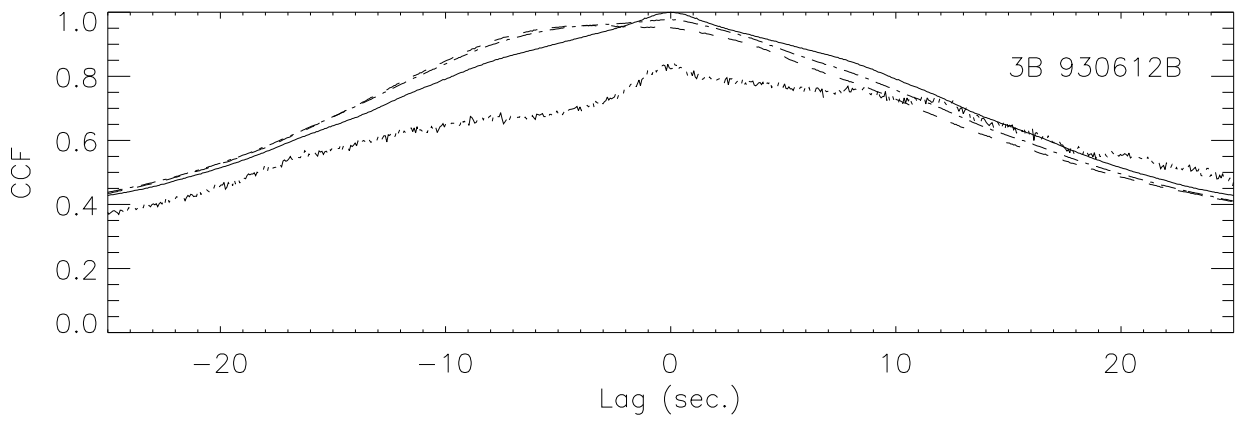
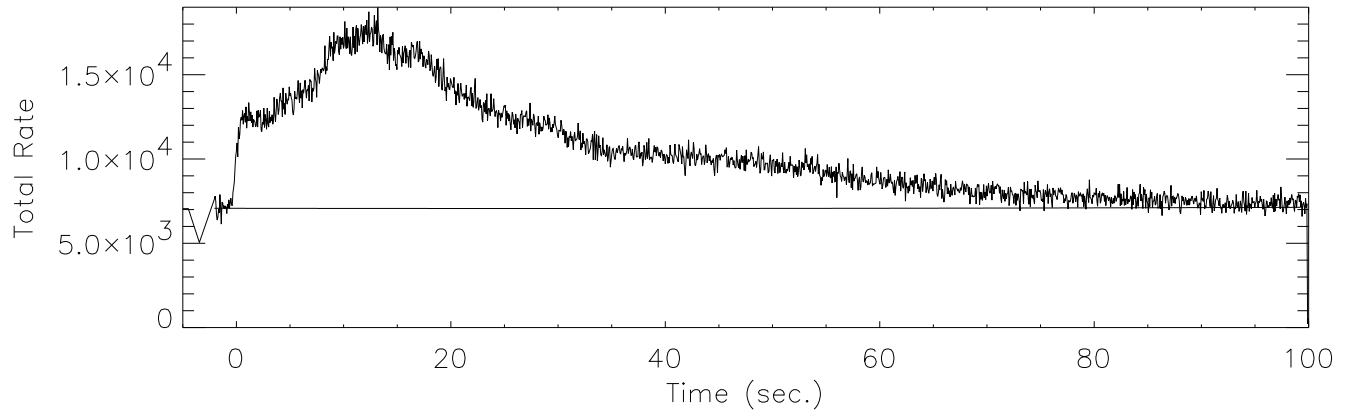


3B 910503





3B 930612B



GB 941119

